Mock LISA Data Challenge 1B: $\mathcal{F}$-statistic Search for white-dwarf binaries

Note for results submission

Reinhard Prix* John T Whelan† Deepak Khurana

Thu Dec 6 20:05:02 2007 +0100
commitID: 40d6043903fa7e79a503d98e60585b511e7e4a3a

Contents

1 General search method

We use the $\mathcal{F}$-statistic, a coherent matched-filtering detection statistic first introduced by Jaranowski et al. [4] in the context of the search for continuous-wave signals in ground based detectors. This method has been implemented by the LIGO Scientific collaboration in LAL/LALApps [6], and is currently used in the search for quasi-periodic GW signals from spinning neutron stars (e.g. see [1]). The generalization of the $\mathcal{F}$-statistic to a coherent multi-detector search was first obtained by Cutler and Schutz [3]. The application of the $\mathcal{F}$-statistic to the search of continuous-wave sources (such as galactic white-dwarf binaries) using LISA was first discussed in Królak et al. [5].

The multi-detector $\mathcal{F}$-statistic has been implemented in LALapps, in the code `ComputeFStatistic_v2`, which we are using for the present analysis. This is the same method and code that has been used previously by the PrixWhelanAEI group on MLDC1 [2, 7] and MLDC2 [10].

*reinhard.prix@aei.mpg.de
†john.whelan@aei.mpg.de

1.1 Multi-detector $\mathcal{F}$-statistic

As shown in [4], the dimensionless strain signal $s^I(t)$ of a continuous gravitational wave at detector I can be represented in the form

$$s^I(t) = \sum_{\mu=1}^{4} \mathcal{A}^\mu \, h_\mu^I(t) \,, \tag{1.1.1}$$

in terms of four signal-amplitudes $\mathcal{A}^\mu$, which are independent of the detector I, and the detector-dependent basis waveforms $h_\mu^I(t)$. The four amplitudes A^μ can be expressed in terms of two polarization amplitudes A_+, $A_\times$, the initial phase ϕ_0 in the solar-system barycenter (SSB) at a reference time τ_{ref}, and the polarization angle ψ of the wave frame with respect to the equatorial coördinate system, namely

$$\mathcal{A}^1 = \; A_+ \cos\phi_0 \cos 2\psi - A_\times \sin\phi_0 \sin 2\psi \,, \tag{1.1.2a}$$
$$\mathcal{A}^2 = \; A_+ \cos\phi_0 \sin 2\psi + A_\times \sin\phi_0 \cos 2\psi \,, \tag{1.1.2b}$$
$$\mathcal{A}^3 = -A_+ \sin\phi_0 \cos 2\psi - A_\times \cos\phi_0 \sin 2\psi \,, \tag{1.1.2c}$$
$$\mathcal{A}^4 = -A_+ \sin\phi_0 \sin 2\psi + A_\times \cos\phi_0 \cos 2\psi \,. \tag{1.1.2d}$$

We can further relate the two polarization amplitudes A_+ and $A_\times$ to the overall amplitude h_0 and the inclination angle ι of the quadrupole rotation axis with respect to the line of sight, namely

$$A_+ = \frac{1}{2} h_0 \, \left(1 + \cos^2\iota\right) \,, \quad A_\times = h_0 \cos\iota \,. \tag{1.1.3}$$

The four basis waveforms $\{h_\mu^I(t)\}$ are the responses generated in detector I by

$$\overleftrightarrow{h}_1(\tau) = \overleftrightarrow{\varepsilon}_+(\widehat{k}) \cos\phi(\tau) \,, \tag{1.1.4a}$$
$$\overleftrightarrow{h}_2(\tau) = \overleftrightarrow{\varepsilon}_\times(\widehat{k}) \cos\phi(\tau) \,, \tag{1.1.4b}$$
$$\overleftrightarrow{h}_3(\tau) = \overleftrightarrow{\varepsilon}_+(\widehat{k}) \sin\phi(\tau) \,, \tag{1.1.4c}$$
$$\overleftrightarrow{h}_4(\tau) = \overleftrightarrow{\varepsilon}_\times(\widehat{k}) \sin\phi(\tau) \,. \tag{1.1.4d}$$

where $\{\overleftrightarrow{\varepsilon}_A(\widehat{k}) | A = +, \times\}$ is the traceless polarization basis transverse to the propagation direction $\widehat{k}$ and τ is the time that the wave arrives at the solar system barycenter. The precise relationship between the $\{h_\mu^I(t)\}$ and the $\{\overleftrightarrow{h}_\mu(\tau)\}$, and the former's more familiar description in terms of the antenna-pattern functions $a^I(t)$ and $b^I(t)$ [4]) depend on the response of the detector to gravitational waves, and we consider them more carefully in Section 2.2 of this note.

The $\{h_\mu^I(t)\}$ depend on the intrinsic parameters ω of the signal. In the case of continuous waves from isolated neutron stars, ω would only consist of the $s+1$ spin parameters, i.e. $\omega = \{f^{(k)}\}_{k=0}^s$, where $f^{(k)}$ is the k-th time-derivative of the intrinsic signal frequency in the SSB.

In the following we denote the set of "Doppler parameters" (i.e. the parameters affecting the time evolution of the phase) by $\lambda \equiv \{\widehat{k}, \omega\}$, as opposed to the four "amplitude parameters" $\{\mathcal{A}\}^\mu = \mathcal{A}^\mu$.

Using the multi-detector notation of [3, 5], we write vectors in "detector-space" in boldface, i.e. $\{\boldsymbol{s}\}^I = s^I$, and so the signal model (1.1.1) can be written as

$$\boldsymbol{s}(t;\mathcal{A},\lambda) = \mathcal{A}^\mu\, \boldsymbol{h}_\mu(t;\lambda)\,, \tag{1.1.5}$$

with implicit summation over repeated amplitude indices, $\mu \in \{1,2,3,4\}$.

The multi-detector scalar product is defined as

$$(\boldsymbol{x}|\boldsymbol{y}) \equiv \int_{-\infty}^{\infty} \widetilde{x}^I(f)\, S^{-1}_{IJ}(f)\, \widetilde{y}^{J*}(f)\, df\,, \tag{1.1.6}$$

where $\widetilde{x}(f)$ denotes the Fourier transform of $x(t)$. We use implicit summation over repeated detector indices, and the inverse noise matrix is defined by $S^{-1}_{IJ}\, S^{JK} = \delta^K_I$, in terms of the double-sided noise PSD matrix S^{IJ}. In the case of uncorrelated noise, where $S^{IJ} = S^I\, \delta^{IJ}$, the scalar product simplifies to

$$(\boldsymbol{x}|\boldsymbol{y}) = \sum_I (x^I|y^I)\,, \tag{1.1.7}$$

in terms of the usual single-detector scalar product

$$(x^I|y^I) \equiv \int_{-\infty}^{\infty} \frac{\widetilde{x}^I(f)\, \widetilde{y}^{I*}(f)}{S^X(f)}\, df\,. \tag{1.1.8}$$

With the signal model (1.1.1), the log-likelihood ratio is found as

$$\ln \Lambda(\boldsymbol{x};\mathcal{A},\lambda) = \mathcal{A}^\mu\, x_\mu - \frac{1}{2}\mathcal{A}^\mu\, \mathcal{M}_{\mu\nu}\, \mathcal{A}^\nu\,, \tag{1.1.9}$$

where we defined

$$x_\mu(\lambda) \;\equiv\; (\boldsymbol{x}|\boldsymbol{h}_\mu)\,, \tag{1.1.10}$$

$$\mathcal{M}_{\mu\nu}(\lambda) \;\equiv\; (\boldsymbol{h}_\mu|\boldsymbol{h}_\nu)\,. \tag{1.1.11}$$

We see that the likelihood ratio (1.1.9) can be maximized analytically with respect to the unknown amplitudes $\mathcal{A}^\mu$, resulting in the maximum-likelihood estimators

$$\mathcal{A}^\mu_{\mathrm{MLE}} = \mathcal{M}^{\mu\nu}\, x_\nu\,. \tag{1.1.12}$$

Substituting this into the detection statistic, we obtain the so-called $\mathcal{F}$-*statistic*, namely

$$2\mathcal{F}(\boldsymbol{x};\lambda) \equiv x_\mu\, \mathcal{M}^{\mu\nu}\, x_\nu\,, \tag{1.1.13}$$

where $\mathcal{M}^{\mu\nu} \equiv \{\mathcal{M}^{-1}\}^{\mu\nu}$, i.e. $\mathcal{M}_{\mu\alpha}\mathcal{M}^{\alpha\nu} = \delta^\nu_\mu$.

Let us consider the case where the target Doppler parameters λ are perfectly matched to the signal λ_{sig}, we find the expectation value of the $\mathcal{F}$-statistic as

$$E[2\mathcal{F}] = 4 + \mathrm{SNR}^2\,, \tag{1.1.14}$$

in terms of the "optimal" signal-to-noise ratio SNR, which is expressible as

$$\mathrm{SNR}^2 = s_\mu\, \mathcal{M}^{\mu\nu}\, s_\nu = \mathcal{A}^\mu\, \mathcal{M}_{\mu\nu}\, \mathcal{A}^\nu = (\boldsymbol{s}|\boldsymbol{s})\,. \tag{1.1.15}$$

1.2 Parameter estimation

From the expression (1.1.12) for the maximum-likelihood amplitudes $\mathcal{A}^\mu$ in terms of the measured F_a, F_b, we can infer the signal-parameters $A_+, A_\times$ (or equivalently h_0, $\cos\iota$) and ψ, ϕ_0, by using (1.1.3) and (1.1.2). We compute the two quantities

$$A_s^2 \equiv \sum_{\mu=1}^{4} (\mathcal{A}^\mu)^2 = A_+^2 + A_\times^2 \,, \tag{1.2.1}$$

$$D_a \equiv \mathcal{A}^1\mathcal{A}^4 - \mathcal{A}^2\mathcal{A}^3 = A_+\, A_\times \,, \tag{1.2.2}$$

which can easily be solved for A_+, $A_\times$, namely

$$2A_{+,\times}^2 = A_s^2 \pm \sqrt{A_s^4 - 4D_a^2}\,, \tag{1.2.3}$$

where our convention here is $|A_+| \geq |A_\times|$, cf. (1.1.3), and therefore the '+' solution is A_+, and the $'-'$ is $A_\times$. The sign of A_+ is always positive by this convention, while the sign of $A_\times$ is given by the sign of D_a, as can be seen from (1.2.2). Note that the discriminant in (1.2.3) is also expressible as

$$\text{disc} \equiv \sqrt{A_s^4 - 4\,D_a^2} = A_+^2 - A_\times^2 \geq 0\,. \tag{1.2.4}$$

Having computed $A_+, A_\times$, we can now also obtain ψ and ϕ_0, namely defining $\beta \equiv A_\times/A_+$, and

$$b_1 \equiv \mathcal{A}^4 - \beta\mathcal{A}^1\,, \tag{1.2.5}$$

$$b_2 \equiv \mathcal{A}^3 + \beta\mathcal{A}^2\,, \tag{1.2.6}$$

$$b_3 \equiv \beta\mathcal{A}^4 - \mathcal{A}^1\,, \tag{1.2.7}$$

we easily find

$$\psi = \frac{1}{2}\,\text{atan}\left(\frac{b_1}{b_2}\right)\,. \tag{1.2.8}$$

and

$$\phi_0 = \text{atan}\left(\frac{b_2}{b_3}\right)\,. \tag{1.2.9}$$

The amplitudes $\mathcal{A}^\mu$ are seen from (1.1.2) to be invariant under the following gauge-transformation, namely *simultaneously* $\{\psi \to \pi/2,\ \phi_0 \to \phi_0 + \pi\}$. Applying this twice, and taking account of the trivial gauge-freedom by 2π, this also contains the invariance $\psi \to \psi + \pi$. Note that there is still an overall sign-ambiguity in the amplitudes $\mathcal{A}^\mu$, which can be determined as follows: compute a 'reconstructed' $\mathcal{A}_r^1$ from (1.1.2) using the estimates $A_{+,\times}$ and ψ, ϕ_0, and compare its sign to the original estimate $\mathcal{A}^1$ of (1.1.12). If the sign differs, the correct solution is simply found by replacing $\phi_0 \to \phi_0 + \pi$.

In order to fix a unique gauge, we restrict the quadrant of ψ to be $\psi \in [-\pi/4, \pi/4)$ (in accord with the TDS convention), which can always be achieved by the above gauge-transformation, while ϕ_0 remains unconstrained in $\phi_0 \in [0, 2\pi)$.

Converting $A_+, A_\times$ into h_0 and $\mu \equiv \cos\iota$ is done by solving (1.1.3), which yields

$$h_0 = A_+ + \sqrt{A_+^2 - A_\times^2}\,, \tag{1.2.10}$$

where we only kept the '+' solution, as we must have $h_0 > A_+$. Finally, $\mu = \cos\iota$ is simply given by $\cos\iota = A_\times/h_0$.

We know that the errors dx_μ satisfy (assuming Gaussian noise):

$$E[dx_\mu\, dx_\nu] = \mathcal{M}_{\mu\nu}\,. \tag{1.2.11}$$

As a consequence of (1.1.12), we therefore obtain the covariance-matrix of the estimation-errors $d\mathcal{A}^\mu$ as

$$E[d\mathcal{A}^\mu\, d\mathcal{A}^\nu] = \mathcal{M}^{\mu\nu}\,, \tag{1.2.12}$$

which corresponds to the Cramér-Rao bound, and $\mathcal{M}^{\mu\nu}$ is seen to be the inverse Fisher-matrix. The corresponding Fisher matrix for the variables $\{h_0, \cos\iota, \psi, \phi_0\}$ is simply obtained from the above together with the appropriate Jacobian accounting for the variables-transformation from $\mathcal{A}^\mu$.

2 Application to LISA and our MLDC pipeline

2.1 MLDC conventions for amplitude parameters

Unfortunately, the MLDC conventions for the amplitude parameters differ from the above standard LIGO/CW definitions for $\{h_0, \cos\iota, \psi, \phi_0\}$. Here we only summarize without derivation how the "translation" is performed:

- MLDC "Amplitude" $= h_0/2$
- MLDC "Inclination" $= \pi - \iota$
- MLDC "Polarization" $= \pi/2 - \psi$
- MLDC "InitialPhase" $= \phi_0$

Note: There still seems to be an overall sign-difference (corresponding to a difference of π in the "InitialPhase") between our estimated amplitude-parameters and those quoted in the MLDC keys, which is not understood. This sign-differences was already noted in MLDC1 and MLDC2 and appears to be still present in MLDC1B, we therefore simply "correct" our quoted "InitialPhase" by π.

2.2 TDI Response and Fourier Approximation

Our analysis is performed in the frequency domain, but we have to account for the fact that the Doppler-shifted frequency of the signal and the detector response will vary gradually over the full one-year observation time in MLDC1B. We deal with this by breaking up the full year into shorter intervals and performing short-time Fourier transforms (SFTs) over

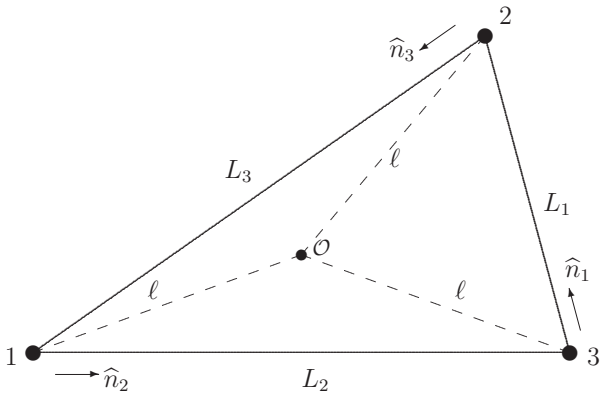

Figure 1: LISA configuration and TDI conventions used.

which the spectral properties and detector geometry can be treated as constant. This is the same method used in the LSC for ground-based continuous wave (CW) searches, where a typical SFT time is 30 minutes. For the MLDCs, we have used one-week SFTs. During the αth time interval, we assume the detector output is adequately described by the αth SFT:

$$h^I(t \in \mathcal{T}_\alpha) \approx h^I_\alpha(t) = \int_{-\infty}^{\infty} df\, \widetilde{h}^I_\alpha(f)\, e^{i2\pi ft} \ . \tag{2.2.1}$$

It is convenient to regard the signal contribution to the SFT of the raw data associated with a particular TDI variable as being related to the strain $\widetilde{h}^I_\alpha(f)$ by a frequency-domain response function $R_\alpha(f)$:

$$\widetilde{q}^X_\alpha(f) = \frac{\widetilde{h}^I_\alpha(f)}{R_\alpha(f)} = \frac{\overleftrightarrow{h}_\alpha(f) : \overleftrightarrow{d}^I_\alpha(f,\widehat{k})}{R_\alpha(f)} \ . \tag{2.2.2}$$

This division allows us to

- Use a different scalar response function $R(f)$ for LISAsim and synthLISA, but the same response tensor $\overleftrightarrow{d}$
- Convert the full data stream, including noise, non-WDB signals, and WDBs at all sky locations to "strain" using a single $R(f)$

For example, for the TDI X variable in LISA simulator, the frequency-domain response in the rigid adiabatic (RA) approximation is (see Figure 1)[8]

$$\begin{aligned}
\frac{\overleftrightarrow{d}^X_\alpha(f,\widehat{k})}{R^{\rm LISAsim}(f)} &= e^{-i2\pi fL(6-\widehat{k}\cdot\widehat{n}_2+\widehat{k}\cdot\widehat{n}_3)/3c}\left(-i\frac{4\pi fL}{c}\right)\mathrm{sinc}\left(\frac{2\pi fL}{c}\right) \\
&\times\left\{\frac{\widehat{n}_2\otimes\widehat{n}_2}{2}\Big[e^{i\frac{\pi fL}{c}(1-\widehat{k}\cdot\widehat{n}_2)}\,\mathrm{sinc}\left(\frac{\pi fL}{c}[1+\widehat{k}\cdot\widehat{n}_2]\right)+e^{-i\frac{\pi fL}{c}(1+\widehat{k}\cdot\widehat{n}_2)}\,\mathrm{sinc}\left(\frac{\pi fL}{c}[1-\widehat{k}\cdot\widehat{n}_2]\right)\Big]/2\right. \\
&\left.-\frac{\widehat{n}_3\otimes\widehat{n}_3}{2}\Big[e^{i\frac{\pi fL}{c}(1+\widehat{k}\cdot\widehat{n}_3)}\,\mathrm{sinc}\left(\frac{\pi fL}{c}[1-\widehat{k}\cdot\widehat{n}_3]\right)+e^{-i\frac{\pi fL}{c}(1-\widehat{k}\cdot\widehat{n}_3)}\,\mathrm{sinc}\left(\frac{\pi fL}{c}[1+\widehat{k}\cdot\widehat{n}_3]\right)\Big]/2\right\}
\end{aligned} \tag{2.2.3}$$

To lowest order in frequency, in the long-wavelength (LW) limit, the division is obvious:

$$R^{\mathrm{LISAsim\,LW}}(f) = \left(i\frac{c}{4\pi fL}\right) \tag{2.2.4}$$

$$\overleftrightarrow{d}{}^{X\,\mathrm{LW}}_{\alpha} = \frac{\widehat{n}_2 \otimes \widehat{n}_2}{2} - \frac{\widehat{n}_3 \otimes \widehat{n}_3}{2} \tag{2.2.5}$$

This was the form used in the PrixWhelanAEI entries for MLDC1 and MLDC2. The factorization of the full rigid adiabatic response is a matter of convention, but one which keeps the tensor response balanced under inversion of the sky direction $-\widehat{k}$ is

$$R^{\mathrm{LISAsim\,RA}}(f) = R^{\mathrm{LISAsim\,LW}}(f)\, e^{i4\pi fL/c} \left[\mathrm{sinc}\left(\frac{2\pi fL}{c}\right)\right]^{-1} \tag{2.2.6}$$

$$\begin{aligned}
&\overleftrightarrow{d}{}^{X\,\mathrm{RA}}_{\alpha}(f,\widehat{k}) = e^{-i2\pi fL(-\widehat{k}\cdot\widehat{n}_2+\widehat{k}\cdot\widehat{n}_3)/3c} \\
&\times\left\{\frac{\widehat{n}_2\otimes\widehat{n}_2}{2}\left[e^{i\frac{\pi fL}{c}(1-\widehat{k}\cdot\widehat{n}_2)}\,\mathrm{sinc}\left(\frac{\pi fL}{c}[1+\widehat{k}\cdot\widehat{n}_2]\right)+e^{-i\frac{\pi fL}{c}(1+\widehat{k}\cdot\widehat{n}_2)}\,\mathrm{sinc}\left(\frac{\pi fL}{c}[1-\widehat{k}\cdot\widehat{n}_2]\right)\right]/2\right. \\
&\left.-\frac{\widehat{n}_3\otimes\widehat{n}_3}{2}\left[e^{i\frac{\pi fL}{c}(1+\widehat{k}\cdot\widehat{n}_3)}\,\mathrm{sinc}\left(\frac{\pi fL}{c}[1-\widehat{k}\cdot\widehat{n}_3]\right)+e^{-i\frac{\pi fL}{c}(1-\widehat{k}\cdot\widehat{n}_3)}\,\mathrm{sinc}\left(\frac{\pi fL}{c}[1+\widehat{k}\cdot\widehat{n}_3]\right)\right]/2\right\}
\end{aligned} \tag{2.2.7}$$

The response tensors for the Y and Z TDI variables can be obtained by cyclic permutations of the unit vectors $\widehat{n}_1$, $\widehat{n}_2$, and $\widehat{n}_3$, and response tensors for linear combinations like $Y - Z$ are simply the appropriate linear combinations of the corresponding response tensors.

Technically, the implementation of the scalar response function $R^{\mathrm{RA}}(f)$ is simpler than that of the response tensor $\overleftrightarrow{d}{}^{\mathrm{RA}}_{\alpha}(f,\widehat{k})$. Therefore, shortly after the submission of our MLDC2 entry, we developed the partial rigid adiabatic approach, using SFTs calibrated with $R^{\mathrm{RA}}(f)$ in conjunction with $\overleftrightarrow{d}{}^{\mathrm{LW}}$. This already produced a marked improvement in the estimation of amplitude parameters.[9, 10]

We distinguish among four different approximations, as summarized in Table 1. Comparisons between approximations showed the effectiveness of our improved response modelling. The submitted results used the full rigid adiabatic (RA) response.

Given the response tensor, we're able to construct the frequency-domain template waveforms:

$$h^I_{\alpha,1}(f) = a^I_\alpha(f,\widehat{k})\,\widetilde{\cos\phi}(f)\ , \tag{2.2.8a}$$

$$h^I_{\alpha,2}(f) = b^I_\alpha(f,\widehat{k})\,\widetilde{\cos\phi}(f)\ , \tag{2.2.8b}$$

$$h^I_{\alpha,3}(f) = a^I_\alpha(f,\widehat{k})\,\widetilde{\sin\phi}(f)\ , \tag{2.2.8c}$$

$$h^I_{\alpha,4}(f) = b^I_\alpha(f,\widehat{k})\,\widetilde{\sin\phi}(f) \tag{2.2.8d}$$

where the AM coëfficients are constructed from the response tensor according to

$$a^I_\alpha(f,\widehat{k}) = \overleftrightarrow{d}{}^I_\alpha(f,\widehat{k}) : \overleftrightarrow{\varepsilon}_+(\widehat{k}) \tag{2.2.9a}$$

$$b^I_\alpha(f,\widehat{k}) = \overleftrightarrow{d}{}^I_\alpha(f,\widehat{k}) : \overleftrightarrow{\varepsilon}_\times(\widehat{k})\ . \tag{2.2.9b}$$

Note the differences from the long-wavelength AM coëfficients:

Table 1: Different approximations used in modelling TDI response. The long-wavelength limit (LWL) was used in our MLDC1 and MLDC2 entries. Partial rigid adiabatic (RA), which uses RA SFTs with the LW response tensor, was applied to MLDC2 shortly after submission. For MLDC1B we have implemented the RA response tensor, allowing us use the full rigid adiabatic response. A more approximate but faster approach, known as *buffered RA* calculates the response tensor once per sky position, using the central frequency $f_{\rm cent}$ of the frequency band being analyzed. This can be sufficiently accurate if the analysis is divided up into narrow enough frequency bands.

Approx	$R(f)$	$\overleftrightarrow{d}(f,\widehat{k})$
LWL	$R^{\rm LW}(f)$	$\overleftrightarrow{d}^{\rm LW}$
partial RA	$R^{\rm RA}(f)$	$\overleftrightarrow{d}^{\rm LW}$
full RA	$R^{\rm RA}(f)$	$\overleftrightarrow{d}^{\rm LW}(f,\widehat{k})$
buffered RA	$R^{\rm RA}(f)$	$\overleftrightarrow{d}^{\rm LW}(f_{\rm cent},\widehat{k})$

- The a and b now depend on frequency as well as sky position.
- The time dependence usually ascribed to a and b is represented by the SFT index α.
- The a and b are now complex, thanks to the complex response tensor.

2.2.1 Amplitude Parameter Metric

The amplitude parameter metric elements

$$\mathcal{M}_{\mu\nu} = \sum_{\alpha}\sum_{I}\int_{-\infty}^{\infty} df\, \frac{\widetilde{h}^I_{\alpha,\mu}(f)^*\,\widetilde{h}^I_{\alpha,\nu}(f)}{S^I_\alpha(f)} \tag{2.2.10}$$

are complicated slightly by the complex nature of a and b. We end up with

$$\{\mathcal{M}_{\mu\nu}\} = \begin{pmatrix} A & C & 0 & E \\ C & B & -E & 0 \\ 0 & -E & A & C \\ E & 0 & C & B \end{pmatrix}\,, \tag{2.2.11}$$

where

$$A = \sum_{\alpha}\sum_{I} \frac{S^I_\alpha(f_0)^{-1}T_{\rm SFT}}{2}\left|a^I_\alpha(f_0)\right|^2 \tag{2.2.12a}$$

$$B = \sum_{\alpha}\sum_{I} \frac{S^I_\alpha(f_0)^{-1}T_{\rm SFT}}{2}\left|b^I_\alpha(f_0)\right|^2 \tag{2.2.12b}$$

$$C = \sum_{\alpha}\sum_{I} \frac{S^I_\alpha(f_0)^{-1}T_{\rm SFT}}{2}\,{\rm Re}[a^I_\alpha(f_0)^* b^I_\alpha(f_0)] \tag{2.2.12c}$$

$$E = \sum_{\alpha}\sum_{I} \frac{S^I_\alpha(f_0)^{-1}T_{\rm SFT}}{2}\,{\rm Im}[a^I_\alpha(f_0)^* b^I_\alpha(f_0)]\,. \tag{2.2.12d}$$

Its inverse is

$$\{\mathcal{M}^{\mu\nu}\} = \frac{1}{D}\begin{pmatrix} B & -C & 0 & -E \\ -C & A & E & 0 \\ 0 & E & B & -C \\ -E & 0 & -C & A \end{pmatrix} , \tag{2.2.13}$$

where we have defined the determinant

$$D = AB - C^2 - E^2 \tag{2.2.14}$$

These generalizations have now been built into the LAL/LALApps code.

2.3 Wide-parameter search grid

For simplicity we used a "foliated" template grid `Freq x Sky` in the Doppler parameter space $\Delta\lambda = \{f, \alpha, \delta\}$, consisting of a *isotropic* sky-grid with step-sizes at the equator:

$$d\alpha(0) = d\delta = \frac{\sqrt{2m}}{(R_{\rm orb}/c)2\pi\, f} , \tag{2.3.1}$$

while for different latitudes we'll use $d\alpha(\delta) = d\alpha(0)/\cos(\delta)$, in order to obtain an isotropic sky-grid. The frequency step-size is given by

$$df = \frac{\sqrt{12m}}{\pi\, T} , \tag{2.3.2}$$

where m is the desired maximal mismatch, f is the search-frequency and T the length of observation. The expression for the frequency-resolution is the standard metric frequency stepsize, while the sky-resolution is approximately valid for observation times $T \gtrsim 1/2\,\mathrm{yr}$, and can be derived from the orbital phase-metric.

2.4 MLDC1B WDB Pipeline

The basic structure of the MLDC1B pipeline was the same as that used in MLDC2, making extensive use of the parameter-space metric for finding local maxima and deciding coïncidences. Furthermore, this pipeline and its parameter-tuning were specifically designed to reduce secondary maxima and allow mostly primary candidates to pass. This is based on the empirical observation that the location of secondary maxima seems to vary more strongly between 'detectors' X, Y and Z than the maxima corresponding to primary candidates, especially if an integration time of only $T = 1\,\mathrm{yr}$ is used.

The parameters that were used with this pipeline are:

grid-mismatch in 1st-stage wide-parameter searc
1st-stage detection threshold
metric sphere for local-maxima
coarse-coïncidence mismatch
tight-coïncidence mismatch
resolution-increase in each zoom
number of final zoom-steps

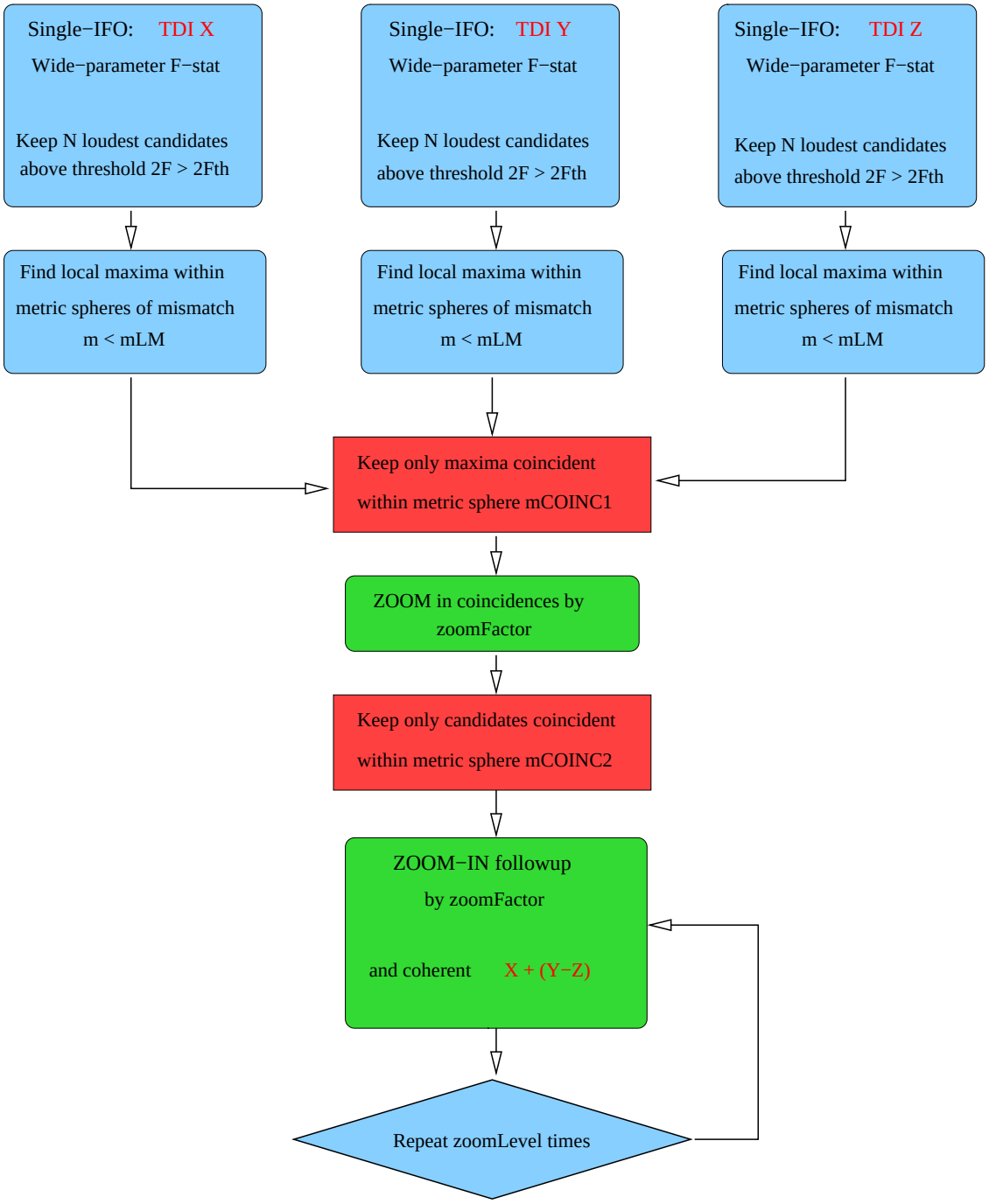

Figure 2: Schematic representation of wide-parameter pipeline used in MLDC1B.

Using these parameters, the pipeline performs reasonably well in reducing "false alarms" due to secondary maxima. However, this scheme does not appear to deal well with highly confused sources. This is illustrated by the decreasing detection efficiency between 1B.1.4 (13 sources found) and 1B.1.5 (only 3 sources found). More work is required to deal with the confusion problem in a more satisfactory way.

References

[1] B. Abbott et al. Coherent searches for periodic gravitational waves from unknown isolated sources and Scorpius X-1: results from the second LIGO science run. *Phys. Rev. D.*, 76:082001, 2007. (LIGO Scientific Collaboration).

[2] K. A. Arnaud et al. *Class. Quant. Grav.*, 24:S529–S539, 2007.

[3] C. Cutler and B. F. Schutz. The generalized F-statistic: multiple detectors and multiple gravitational wave pulsars. *Phys. Rev. D.*, 72:063006, 2005.

[4] P. Jaranowski, A. Królak, and B. F. Schutz. Data analysis of gravitational-wave signals from spinning neutron stars: The signal and its detection. *Phys. Rev. D.*, 58:063001, 1998.

[5] A. Królak, M. Tinto, and M. Vallisneri. Optimal filtering of the LISA data. *Phys. Rev. D.*, 70:022003, 2004.

[6] LIGO Scientific Collaboration. LAL/LALApps: FreeSoftware (GPL) tools for data-analysis. `http://www.lsc-group.phys.uwm.edu/daswg/`.

[7] R. Prix and J. T. Whelan. F-statistic search for white-dwarf binaries in the first Mock LISA Data Challenge. *Class. Quant. Grav.*, 24:S565–S574, 2007.

[8] L. J. Rubbo, N. J. Cornish, and O. Poujade. Forward modeling of space-borne gravitational wave detectors. *Phys. Rev. D.*, 69(8):082003–+, Apr. 2004. doi: 10.1103/PhysRevD.69.082003.

[9] J. T. Whelan. F-Statistic Searches for White Dwarf Binaries in the Mock LISA Data Challenges. LIGO-G070778-00-Z, 2007. Seminar at the University of Wales, Cardiff.

[10] J. T. Whelan, R. Prix, and D. Khurana. Second Mock LISA Data Challenge: search for galactic white dwarf binaries using an $\mathcal{F}$-statistic template bank. 2008.